41

Imaging Brain Slices

Ayumu Tashiro, Gloster Aaron, Dmitriy Aronov, Rosa Cossart, Daniella Dumitriu, Vivian Fenstermaker, Jesse Goldberg, Farid Hamzei-Sichani, Yuji Ikegaya, Sila Konur, Jason MacLean, Boaz Nemet, Volodymyr Nikolenko, Carlos Portera-Cailliau, and Rafael Yuste

INTRODUCTION

Brain slices are convenient preparations to study synapses, neurons, and neural circuits because, while they are easily accessed by experimental manipulations such as drug applications, intracellular recordings, and optical imaging, they preserve many of the essential functional properties of these circuits. In this chapter, we describe techniques of live brain-slice imaging used in our laboratory. We cover in detail experimental protocols and know-how acquired over the years about preparing neocortical and hippocampal slices and slice cultures, loading neurons with dyes or using biolistic transfection techniques, two-photon and second harmonic imaging, morphological reconstructions, and image processing and analysis. These techniques are used to study the functional or morphological dynamics of synaptic structures, including dendritic spines and axon terminals, and to characterize circuit connectivity and dynamics.

The importance of developing methods is underestimated in modern biology. The education of biomedical researchers and the federal granting agencies are dominated by the ideology that good research is question-driven, whereas technique-driven research is of lesser quality. We disagree with this exclusive view because it seems to us that the specific technique used is as important as the question addressed. As Sydney Brenner put it: "Progress in science depends on new techniques, new discoveries, and new ideas, probably in that order." (Brenner, 2002). As an example, we would argue that the invention of high-affinity, selective calcium indicators have revolutionized many fields of biology (Grynkiewicz *et al*., 1985; Tsien, 1989).

We feel that methods are essential, not only for performing and validating experiments, but as exploratory tools that generate new ideas, leading into new fields. Moreover, in our experience, the difference between a difficult experiment working or not often depends on minute technical details. These details are normally acquired with great effort by the investigator, yet generally they must be left out of publications. To help compensate for this, we present in this chapter a detailed account of current methods used in our laboratory to image living brain slices. The general goal of our work is to use brain tissue specimens thin enough so that they can be successfully imaged optically. As explained in detail below, we use different types of brain slices and keep them in submerged chambers, where we seek to preserve ideal conditions of temperature, ionic composition, and nutrients to enable the slices to survive as long as possible. Slices are imaged normally in upright microscopes, in order to enable electrical, as well as optical, access to the surface of the slice. In this respect, fixed stage microscopes are ideal because they enable the stable positioning of micromanipulators and mechanical independence of the focusing of the objective. Although inverted microscopes enable better optics, they are very difficult to use for electrophysiological experiments with slices because the electrical approach to the preparation comes from the opposite side of the slice than the optical approach.

In this chapter we will discuss a combination of methods to image brain slices that are used in our laboratory. We will first cover in detail the preparation of different types of brain slices, discuss how to label cells in slices with optical probes, and then specifically discuss different types of imaging approaches to slices. We finish with an additional section of useful methods to morphologically reconstruct neurons from slices for histological or ultrastructural work and a brief discussion of different image processing strategies that we use. We hope that other investigators will profit and learn from our experience and that this will enable more research teams to enter the exciting territory of imaging slices.

MAKING BRAIN SLICES

Acute Slices

Acute live slices prepared from the brain have become a standard preparation commonly used to study electrophysiological properties of neurons in circuits (Alger *et al*., 1984) and, more recently, imaging (Yuste, 2000b). Most of our work is carried out with slices from mouse primary visual cortex (Fig. 41.1). The relatively high degree of preservation of neuronal organization after slicing and the availability of a variety of easy experimental manipulations make acute slices an attractive experimental preparation. Generally, acute slices can be maintained in good condition for up to 12 h. At the same time, we find a lot of variability in the quality of slices from day to day and even from slice to slice. The large number of variables that are likely to be important in the preservation of the health of the slice make obtaining good slices somewhat of an art form. Unfortunately, systematic studies to determine

Ayumu Tashiro, Gloster Aaron, Dmitriy Aronov, Rosa Cossart, Daniella Dumitriu, Vivian Fenstermaker, Jesse Goldberg, Farid Hamzei-Sichani, Yuji Ikegaya, Sıla Konur, Jason MacLean, Boaz Nemet, Volodymyr Nikolenko, Carlos Portera-Cailliau, and Rafael Yuste • HHMI, Columbia University, New York, New York 10027

 Handbook of Biological Confocal Microscopy, Third Edition, edited by James B. Pawley, Springer Science+Business Media, LLC, New York, 2006.

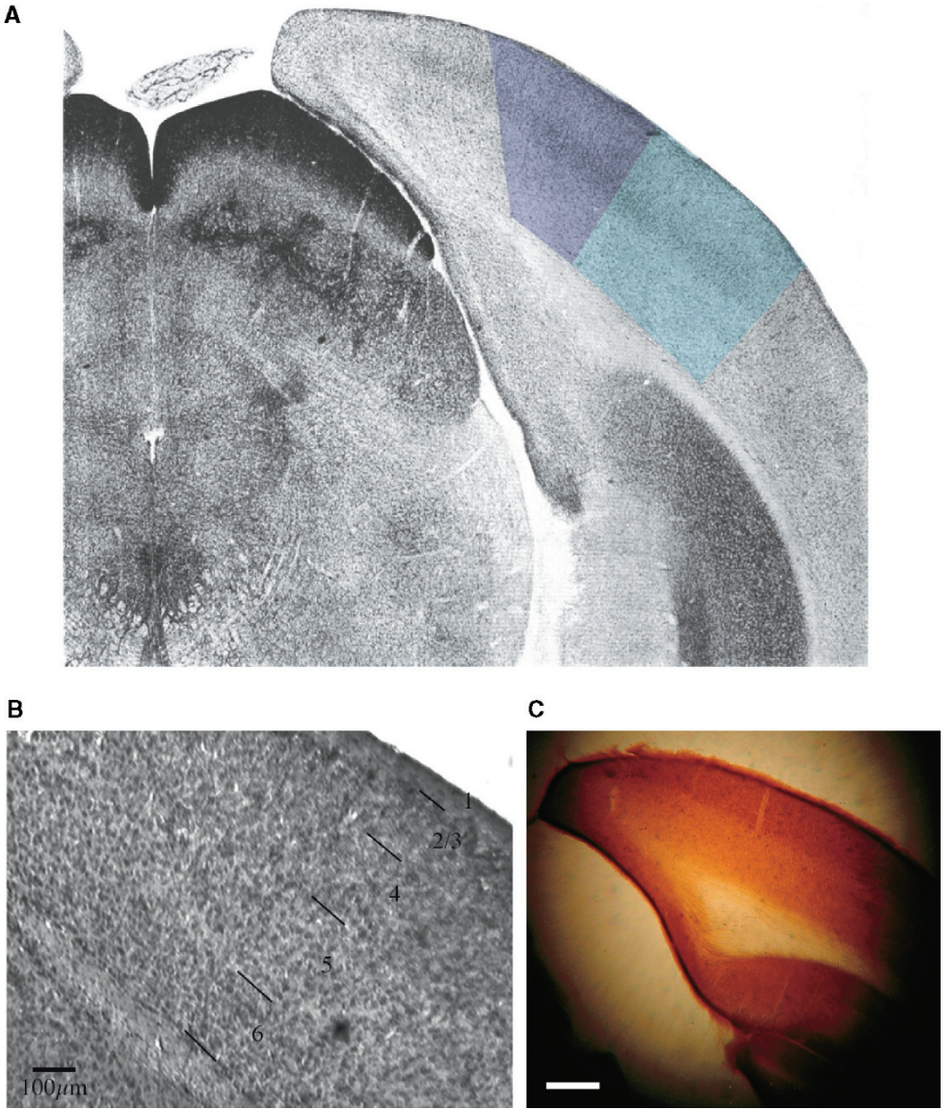

FIGURE 41.1. Brain slices of mouse visual cortex. Representative coronal slices from mouse primary visual cortex. Sections cut through the posterior pole of the cerebral hemisphere. (A) Photomicrograph of an acetylcholinesterase-labeled coronal section taken from the Franklin and Paxinos (1997) atlas. Note the more intense staining in layer 4 due to the high density of small granule cells. Violet and blue shaded areas indicate the monocular and binocular regions of the mouse primary visual cortex, respectively. (B) Nissl stain of a mouse visual cortex slice from a P18 animal. Note the prominent layer 4. (C) Cytochrome oxidase staining of a similar section. Note the intense staining near layer 4, which is an indication of the primary visual cortex. Scale bar = 500 µm. (Courtesy of Z. Peterlin and A. Tsiola.)

which variables are important to make healthy brain slices have not yet been done.

Protocol for Acute Neocortical Slices

Mice are anesthetized with 120 mg/kg ketamine and 10 mg/kg xylazine (intraperitoneally) and decapitated with scissors. Some investigators in our laboratory prefer to perfuse the mouse with a gravity-fed cold saline solution prior to decapitation. The skin covering the skull is severed with a fresh razor blade above the midsaggital line of the skull. The skull is then cut along this line and forceps are slid under the skull posteriorly, such that an air bubble forms anterior to the forceps tips. This air bubble provides a perfect pocket for the forceps to slide anteriorly, with care taken not to touch cortical tissue with the forceps. Each half of the skull may then be retracted laterally. The brain is then exposed and should be immediately placed into ice-cold sucrose artificial cerebrospinal fluid (sucrose-ACSF; 222 m*M* sucrose, 2.6 m*M* KCl, 27 m*M* $NaHCO_3$, 1.5 m*M* NaH_2PO_4, 2 m*M* $CaCl_2$, 2 m*M* $MgSO_4$, bubbled with 95% O_2, 5% CO_2). After approximately 3 min in ice-cold sucrose ACSF, the brain is removed and situated on the cutting block such that the cortex faces the approaching blade. Slices 300 to 400 µm thick are cut with a vibratome (Leica VT1000S; Leica, Nussloch, Germany; high vibration and slow speed setting) and incubated at 37°C for 30 min in a submerged slice chamber. Slices are then incubated at room temperature for up to 12 h, until used for experiments.

Identification of Primary Visual Cortex

The primary visual cortex, or area 17, of the mouse is located in the occipital region of the brain. In the adult animals it extends 1.3 mm anteriorly from the posterior end of the cortex (interaural line). In coronal sections it extends between 1 to 2 mm laterally from the medial line at its anterior border and between 2 to 3 mm in the most posterior (Franklin and Paxinos, 1997). The primary visual cortex of the mouse is divided into two regions: the monocular region, which receives input from the contralateral retina and is located in the medial part, and the binocular region, which receives input from both retinas and is placed laterally (Zilles and Wree, 1985). The primary visual cortex can be identified in coronal sections by the densely arranged granule cells of layer 4 (Fig. 41.1).

Thalamocortical Slice Protocol

Thalamocortical slices are an ideal preparation to investigate the effect of thalamic inputs onto cortical neurons or circuits because it preserves both structures and connections between the ventrobasal nucleus of the thalamus and the somatosensory cortex. Preparation of the thalamocortical slice is slightly modified from Agmon and Connors (1991), as previously described (Beierlein *et al*., 2002). Briefly, C57BL/6 mice postnatal (P) 10 to 18 are anesthetized with 120 mg/kg ketamine and 10 mg/kg xylazine and decapitated. The brain is quickly removed and placed into cold artificial CSF (ASCF) containing the following (in millimolars): 126 NaCl, 3 KCl, 1.25 NaH_2PO_4, 26 $NaHCO_3$, 10 dextrose, 1.3 $MgSO_4$, and 2.5 $CaCl_2$ (saturated with 95% O_2 and 5% CO_2). The brain is midsagittally sectioned into the left and right hemispheres. Each hemisphere is glued (standard cyanacrylate "super" glue) to a plastic block, midline down, anterior end pointing toward the floor and ventral surfaces facing in, toward one another. The hemispheres are rotated 10° from center line of the block. The plastic block is actually a right triangle with the hypotenuse 55° from the level (floor). Slices, 400 µm thick, are cut with a vibratome (VT1000S) and then incubated at 32°C for 45 min. Usually two or three viable thalamocortical slices can be made from each hemisphere.

Cultured Slices

Because acute slices cannot be maintained in good condition for more than 12 h, long-term culture is required for manipulations involving long-term experiments, such as those requiring the expression of genes. Below, we describe the protocol for mouse hippocampal slice cultures, which we have used extensively to image the morphology of single neurons transfected with the green fluorescent protein (GFP) (Dunaevsky *et al*., 1999; Tashiro *et al*., 2000).

Protocol for Hippocampal Cultured Slices

Neonatal mice (P0–P3) are cryoanesthetized on ice for 1 min and decapitated with scissors. In a tissue culture hood, skin and skull are cut with scissors and separated with forceps. The brain is then gently removed and placed into a 35 mm tissue culture dish filled with cold sucrose-ACSF (see above). Under a dissecting microscope, the two hemispheres are separated with a surgical blade and oriented such that the medial surface faces down. The cerebellum and the mesencephalon are carefully dissected away and discarded. Then, after the hemisphere is rotated such that its medial side faces up, the diencephalon is removed with a surgical blade and a flat-ended spatula. The remaining piece of tissue, representing the cortex and the hippocampus, is trimmed into a rectangular block along the anterior edge of the hippocampus parallel to the septotemporal axis. The tissue is transferred onto a tissue chopper (TC-2 Tissue Sectioner; Smith & Farquhar) with two spatulas. The rectangular block of tissue is positioned such that the chopping orientation is perpendicular to the septotemporal axis of the hippocampus. Slices 300 µm thick are obtained. With two flat-ended spatulas, the slices are transferred to a fresh culture dish containing cold sucrose-ACSF. The slices are separated from each other with a surgical blade and a flat-ended spatula as soon as possible.

Slices are cultured in culture medium, 100 mL of which contains 50 mL Basal Medium Eagle (catalog #21010-046, Invitrogen), 25 mL Hank's Balanced Salt Solution (catalog #24020-117, Invitrogen), 25 mL heat-inactivated horse serum (Hyclone), 0.65 g dextrose, 0.5 mL L-glutamine (catalog #25030-149, Invitrogen), 1.0 mL HEPES (catalog #15630-106, Invitrogen), and 1.0 mL 100X Pen-strep (catalog #15140-148, Invitrogen). Approximately 1 mL of medium is poured onto and under the culture inserts (catalog #PICM 030 50 or PICM ORG 50, Millipore) in the sterile hood, so that the membrane of the inserts is completely submerged in culture medium. We find that the use of serum from Hyclone (Logan, UT) is a particularly important variable because cultures made with serum from other sources were not successful. Individual slices are then transferred onto the membrane with a flat-ended spatula. Three to six slices are cultivated on single inserts. Most of the medium (but not all) is removed from the inserts with a pipette, and the slices are positioned with the spatula at the center of the insert, but separated from each other by at least 2 to 3 mm. Then, all remaining medium in the inserts is aspirated. The inserts are transferred into 6-well culture plates, in which each well contains 1 mL of culture medium. The culture plates are kept in the incubator (5% CO_2, 37°C). Every other day, 0.6 mL of culture medium is changed with fresh medium. During the first few days in culture, slices spread slightly and become flattened to a 150 to 250 µm thickness.

LABELING CELLS

Biolistic Transfection

To image neuronal morphology, we transfect GFP using biolistics ("gene gun") (Arnold *et al*., 1994; Lo *et al*., 1994). The principle of this method is that metal particles coated with DNA are transferred physically into nucleus by pressured gas. Transferred GFP genes are expressed and the whole neuronal cytoplasm, including their axons and dendrites, can be visualized (Fig. 41.2).

Biolistic Protocol

We use the Helios Gene Gun System (Bio-Rad), and the following protocol is modified from the procedure described in the manual for the system. Plasmids are purified on a Qiagen Maxiprep kit. Weigh 12.5 mg gold (1 µm diameter) in a 1.5 mL tube and add 100 µL of 0.05 *M* Spermidine. Sonicate the tube for 5 s to dissociate aggregated gold particles (FS30, Fisher Scientific; 40 kHz, 130 W). Add solution containing desired amount of plasmid [for eGFP-C1 plasmid (Clontech), 100 µg] and precipitate plasmid onto gold particles with 100 µL of 1 m*M* $CaCl_2$. In 10 min, gold particles precipitate to the bottom of the tube. Then, remove supernatant solution without disturbing the particles and wash particles three times with 100% EtOH. The particles are then suspended in 100% EtOH and transferred into a new 15 mL tube to a final volume of 3 mL. Transfer particles in EtOH into Tefzel tube (Bio-Rad). In approximately 90 s, gold particles precipitate to

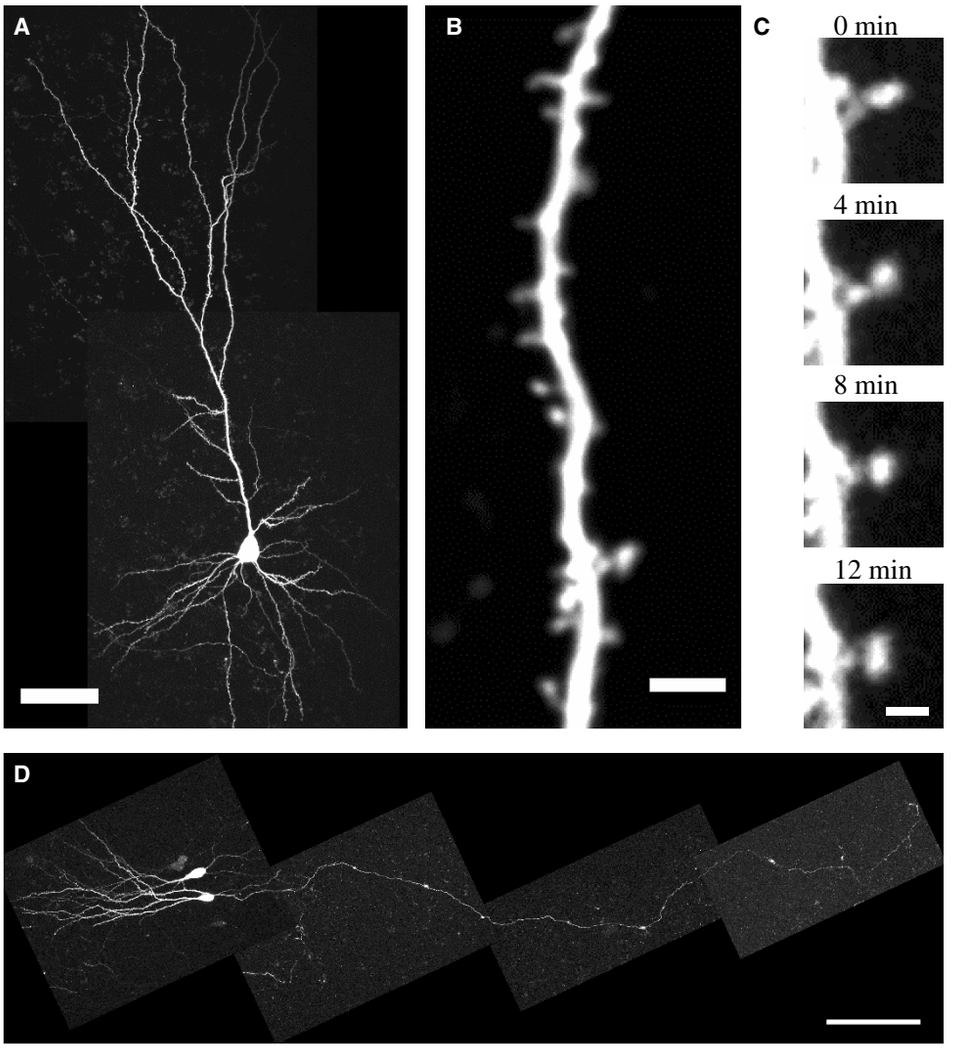

FIGURE 41.2. Two-photon imaging of living neurons in slices. Two-photon micrographs of GFP-transfected neurons in hippocampal brain slice cultures. (A) A CA3 pyramidal neuron at 14 days *in vitro*. (B) Apical dendrite of a CA3 pyramidal neuron at 11 days *in vitro*. (C) Time-lapse sequence of a dendritic spine in (B). Note the morphological rearrangements occurring in a few minutes. (D) Dentate granule cells at 14 days *in vitro*. Note that the entire dendritic and axonal processes are visualized. Scale bar: (A) 50 μm, (B) 2.5 μm, (C) 1 μm. (D) 150 μm.

the bottom of the tube. Then, EtOH is removed from the tube slowly without disturbing the particles. Tube is dried with nitrogen gas until the inside surface of the tube becomes completely dry. With tubing cutter (Bio-Rad), the tube is cut into small pieces, which are used for single shots. Tubing sets can be stored with desiccant at 4°C for up to a month and at −80°C for longer storage.

To drive gold particles into neuronal nuclei, we use high-pressure helium flow. We adjust the helium pressure to 100 to 150 psi for transfection of slice cultures and acute slices. Two to three "preshots" are fired with an empty cartridge holder to clean the helium pathway and make sure that pressure is stable after each shot. In order to reduce the damage to slices caused by high-pressure flow, the tips of barrel liners are covered by a nylon mesh (ϕ90 μm, Small Parts, Inc). For cultured slices, the cover of the culture plate is removed, and the gun is fired perpendicular to the plate with a distance of 10 mm between the tip of the barrel liner and the insert. The culture plates are immediately put back into the incubator. Slices are incubated for 2 to 5 days before imaging.

Genetic Manipulation with Dominant-Negative and Constitutively Active Mutants

One of the advantages of biolistics over other transfection methods is that cotransfection of multiple genes is quite easy. If the two genes are in separate mammalian vectors, they can be cotransfected with high cotransfection efficiency (>90% in our hands) by simultaneously coating gold particles with these two vectors. With cotransfection of GFP and dominant-negative or constitutively active mutant genes, the roles of specific molecular signaling cascades in the regulation of neuronal morphology can be examined. For example, we have been studying the roles of Rho GTPases in

regulating morphology and motility of dendritic spines (Tashiro *et al*., 2000; Tashiro and Yuste, 2004).

Diolistics and Calistics

Conventionally, lipophilic dyes, such as DiO and DiI, are used to label axonal projections between different regions of the brain by placing a crystal of these dyes in a defined region (Honig and Hume, 1989). However, this method is not suitable for imaging the morphology of single neurons because the region near the crystal is stained too densely to visualize single neurons. To label single neurons, Gan and colleagues developed diolistics, a variant of particle-mediated gene transfer, which transfers metal particles coated by fluorescent dyes onto cells (Gan *et al*., 2000). Our group has extensively used this method to visualize neurons in fixed tissue and classified cortical pyramidal neurons in mouse V1 into different morphological categories (Tsiola and Yuste, 2003).

Calistic, another variant of biolistics, serves to inject Ca^{2+} indicators such as calcium green-1 and fura-2 into neuronal cytoplasm (Kettunen *et al*., 2002). With this method, an apparently higher concentration of calcium indicators can be injected into neurons than using acetoxymethyl ester (AM) loading, and a large number of neurons can be visualized. Calistic also allows the simultaneous measurement of morphological and calcium dynamics of single neurons (Lohmann *et al*., 2002).

Dye Injection with Whole-Cell Patch Clamp

Whole-cell patch clamp is commonly used to study electrophysiological properties of neurons in brain slices (Edwards *et al*., 1989). Using electrodes filled with fluorescent dyes, the whole-cell configuration of patch clamp injects the dyes into neurons by diffusion through the pipette tip into the neuron. This technique has the advantages that the labeling procedure is rapid and that any neuron in the slice can be targeted and therefore visualized. When electrophysiological measurements are combined with imaging, a lower concentration of dyes is used and the whole-cell patch clamp is maintained during an experiment (Yuste and Denk, 1995). However, an extended period of patch clamp may interfere with cellular functions such as spine motility (Majewska *et al*., 2000a), possibly because the biochemistry in the neuron is perturbed by the perfusion of intracellular solution or the diffusion of cytoplasm into the patch electrode. Because of this problem, we routinely fill the electrode with higher concentration of fluorescent dyes and pull out the electrode a few minutes after whole cell recording is established (bolus technique, see below; Helmchen *et al*., 1996; Majewska *et al*., 2000a).

Bolus Injection Protocol

Neurons of interest are identified using differential interference contrast (DIC) optics, and then patched and recorded using the whole-cell patch clamp technique in current-clamp configuration to ensure the neurons are healthy. Electrodes are filled with a solution containing (in millimolars): 5 NaCl, 10 KCl, 10 HEPES, 135 $KMeSO_4$, 2.5 to 4 Mg-ATP, 0.3 Na-GTP, and 100 to 500 μ*M* fluorescent dye such as Calcium Green-1 or Alexa-488 (Molecular Probes, Inc., Eugene, OR). Electrodes are then pulled out 1 to 3 min after patching to prevent dialysis of cytoplasm. The resistance of patch electrodes is typically 7 to 14 MΩ. Diffusion of dyes is so rapid that the whole dendritic tree is visualized in a few minutes.

Slice Loading and "Painting" with Acetoxymethyl Ester Indicators

In our past work we have pioneered the use of calcium imaging to characterize the activity of neuronal populations (Yuste and Katz, 1989, 1991; Smetters *et al*., 1999; Peterlin *et al*., 2000). The bulk loading method for double incubation of cortical slices with fura-2 AM or indo-1 AM (Molecular Probes) calcium indicators has been previously described (Yuste and Katz, 1989; Yuste, 2000a). Briefly, cortical slices are initially incubated with 2 to 5 μL of a 1 m*M* fura-2 AM or indo-1 AM in 100% DMSO solution for 2 min, followed by a second incubation in 3 mL of 10 μ*M* fura-2 AM in ACSF for 60 min. However, the use of the thalamocortical slice preparation (Beierlein *et al*., 2002) necessitated the development of a modified bulk-loading procedure because the long-projecting thalamocortical (TC) axons are particularly sensitive to the double incubation methodology, even though local connections within the cortex remain intact (Kozloski *et al*., 2001).

We have been able to circumvent this problem by applying the fura-2 AM or indo-1 AM solution directly to the region of interest in the cortical slice with a pipette, tip diameter approximately 30 μm, filled with fura-2 AM. The region of interest of the slice can be "painted" with fura-2 AM or indo-1 AM. In this way one is able to achieve good loading while preserving TC connections up to postnatal day 18 in mouse barrel cortex (Fig. 41.3). The maintenance of intact TC projections was confirmed using thalamic stimulation that elicits a calcium response in barrel cortex indicative of intact thalamocortical axons (Beierlein *et al*., 2002).

Protocol for Slice AM Painting

1. Deposit TC slice carefully onto the bottom of a small Petri dish (35 × 10 mm) filled with 2 mL of ACSF aspirated with 95% O_2 and 5% CO_2 and place onto microscope stage.
2. Fill a fire-polished pipette (tip diameter ~30 μm) with fura-2 AM from a previously prepared aliquot of 50 μg of fura-2 AM

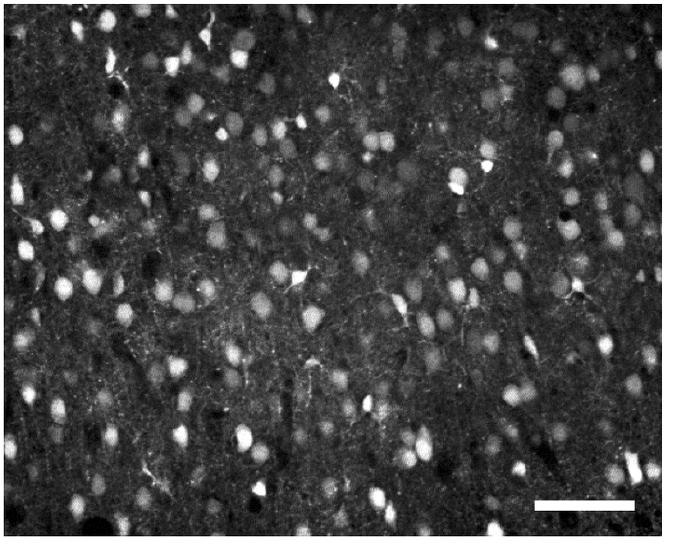

FIGURE 41.3. Two-photon imaging of neuronal ensembles. Two-photon micrograph of an acute cortical brain slice, loaded with indo-1 AM. A number of neurons are loaded with the calcium-sensitive indicator, indo-1. Note that dendritic processes are also visualized in many neurons. 60 pixels correspond to 20 μm. Scale bar: 50 μm.

dissolved in 10 µL of DMSO and 2 µL of pluronic acid (F127, Molecular Probes).
3. Insert the filled pipette into a standard patch clamp electrode holder, with tubing attached, and using a micromanipulator, place pipette tip 100 to 200 µm above the surface of the slice. Apply 5 to 10 psi positive pressure to the pipette. Slowly move the pipette across the surface of the slice using the manipulator, covering the area of interest with the dissolved fura-2 AM.
4. Incubate the slices at 32°C for 24 to 28 min depending on the age of the animal from which the slices were taken (younger animals require shorter incubation times), aspirated with 95% O_2 and 5% CO_2 throughout.
5. Finally transfer the slices to oxygenated ACSF at room temperature at least 15 min before use for the experiment.

Green Fluorescent Protein Transgenic Mice

Recently, a number of different types of GFP transgenic mice have become available commercially or from independent investigators. If these mice express GFP in neurons of interest at the right age, the labeling procedures described above are circumvented. For example, we have used the GFP-M line of GFP transgenic mice developed by Feng and colleagues (Feng *et al*., 2000). At the second postnatal week, this line of mice expresses GFP weakly in V1, but strongly in pyramidal neurons in pyriform cortex. In addition, too many pyramidal neurons in the hippocampal CA1 region are labeled by GFP, so background fluorescence makes it difficult to visualize single neurons.

IMAGING SLICES

Two-Photon Imaging of Slices

For imaging brain slices we almost exclusively use upright microscopes (Olympus BX50WI) because they can provide easy combination of electrophysiological techniques (whole-cell patch clamp and extracellular stimulation) with simultaneous imaging of patched and/or stimulated cells. As explained, with inverted microscopes it is difficult to position the patch/stimulating electrode from one side of the slice and image from the same side. This requirement is satisfied in the case of upright microscope and dipping-type water-immersion objectives with a working distance large enough to enable bringing the electrode in the field of view from the same side.

Two-photon imaging is carried out with a custom-built two-photon laser-scanning microscope (Majewska *et al*., 2000b). A more recent description of our system can be found at www.twophoton.com or at http://www.columbia.edu/cu/biology/faculty/yuste/index.html. The microscope consists of a modified Fluoview (Olympus, Melville, NY) confocal microscope with a titanium : sapphire (Ti : Sa) laser providing ~130 fs pulses at 76 MHz at wavelengths of 700 to 900 nm (Mira, Coherent, Santa Clara, CA) pumped by a solid-state source (Verdi, Coherent). We detect the fluorescence with a non-descanned detector (see below).

Imaging is done at low excitation intensities (3–10 mW at sample). Under these conditions no significant photobleaching or photodamage is observed, allowing us to image for long periods of time. For fast time resolution we can record continuous movies (1000 frames per movie, 0.2–1.6 s/frame), acquiring individual calcium fluorescence signals from hundreds of neurons simultaneously. Alternatively, in a time-lapse mode (1 frame/15 s), we can image the same region for up to 6 h without appreciable photodamage. The major limitation of the use of two-photon imaging to monitor the activity of large neuronal populations is the slow time resolution associated with laser-scanning methods. It is therefore best suited for the study of slow events rather than to detect single spike correlations. By performing online analysis, we can identify prominent features of spontaneous activity, target key elements of the network, perform whole-cell recordings while continuing to image the slice, and characterize electrophysiologically the neurons that participate in these events.

Slice Chamber Protocol

Acute and cultured slices are continuously perfused with standard ACSF containing (in m*M*): 126 NaCl, 3 KCl, 2 $CaCl_2$, 1 $MgSO_4$, 1.1 NaH_3PO_4, 26 $NaHCO_3$, and 10 dextrose and saturated with 95%O_2 and 5%CO_2. To hold the slices on the microscope, we use a temperature-controlled chamber (Series 20 imaging chamber, Warner Instrument). Flow is gravity-driven by raising a container (60 ml syringe, for example) above the chamber and controlled by a flow regulator. ACSF is sucked from the chamber by a vacuum pump. Sometimes it is necessity to use an additional flow regulator in the vacuum line to stabilize the level of liquid in the recording chamber, especially when a powerful vacuum pump ("Air Admiral"; ColeParmer) is used. Medium flow in the chamber can cause movement of the whole slice, which is a serious problem in time-lapse imaging, especially with small structure such as presynaptic and postsynaptic structures. To minimize movement artifacts, medium flow is reduced to 1 ml/min and the slices are stabilized with a slice anchor (Warner Instrument). As an alternative to using a weight that can damage the slice, we also use the direct adherence of the slice to the chamber. To do so, we position the slice on the bottom glass of the chamber and drain all the ACSF. After a few seconds, we reperfuse the chamber carefully so as not to lift the slice. In most cases, the slice has adhered to the chamber and will not move for the rest of the experiment.

ACSF is heated before flowing into the chamber by an in-line heater (SH-27B, Warner Instrument), and the base of the chamber is also heated by a platform heater (Series 20 platform, Warner Instrument). These heaters are controlled by a dual channel heater Controller (TC-344B, Warner Instrument). The temperature of the in-line heater is set at ~39°C and the platform heater is kept at ~39°C, in order to keep the liquid in the chamber at ~36–37C. As an independent control of the liquid temperature, we use an additional thermosensor (Warner) or a thermocouple-based handheld digital thermometer (TES 1300). If ACSF is saturated with O_2 and CO_2 at room temperature, these gases come out of solution in the heated imaging chamber and produce a number of small bubbles. These bubbles degrade image quality and can damage the slices. To prevent this, we keep the ACSF container in a hot bath and saturate the ACSF with the gases at 37°C.

Choice of Objectives

We use 40× (0.8NA) or 60× (0.9NA) dipping-type water immersion objectives (Olympus), although we have recently started to use the new 20× 0.95 NA objective (Olympus) to image a larger number of cortical neurons. With this low-magnification, high-numerical aperture (NA) objective, we can simultaneously monitor the activity of large neuronal populations (average 650 neurons, range 184–1396) in a thin optical section of the slice. The area

viewed covers up to 5 different layers of the primary visual cortex (~400 × 700 μm). The improved depth penetration and the high sensitivity of two-photon imaging allows us to image at depths of >100 μm from the slice surface, where connectivity is less affected by the slicing procedure. High-NA objectives further increase the fluorescence collection and thus allow deeper fluorescence measurements with good resolution than conventional objectives. Even at low magnification, we can resolve individual neurons and some of their dendritic processes. However, a major difficulty associated with the use of the 20× objective for patching, stems from its large dimensions, which restricts access for electrodes.

In general, it is also necessary to minimize the working depth in the tissue. Deeper imaging leads to loss of excitation light and fluorescence signal because of light scattering by the tissue. Also deeper imaging leads to lower contrast in bright-field and makes patching extremely difficult. That is why one of the major requirements for objectives is a long working distance. The Olympus 20×, 40× and 60× water-immersion objectives satisfy this requirement, with working distances of at least 2 mm. On the other hand it is possible to use objectives with shorter working distances for studies which do not require simultaneous imaging and electrophysiological recording (morphological studies of cells labeled genetically or by bolus injection).

The efficiency of signal collection in the case of two-photon laser scanning microscopy using the whole-area detection mode directly depends on the NA of the objective lens used. Also, a higher NA decreases the diffraction-limited size of the excitation spot, which gives better spatial resolution and provides higher local intensity of the excitation light, thus increasing the efficiency of nonlinear optical effects (multi-photon absorption or second-harmonic generation). In this respect, the Olympus 20× 0.95 NA water-immersion objective was crucial and allows 2P Ca^{2+} imaging of large neuronal populations with excellent signal to noise ratio (Fig. 41.3A).

Choosing the right magnification for the objective lens is another practical issue. Lower magnification is good for imaging larger structures; although low-magnification objectives are not convenient for simultaneous electrophysiological recordings, if cells have to be patched while visualizing them through the eyepieces. In some cases, increasing magnification with a separate system of lenses solves this problem. As an example, we have a "U-CA" adaptor from Olympus for the BX 50WI microscope, which works as a magnifying telescope and is inserted into the optical pathway of the microscope in the region where the light is collimated. On the other hand it is not ideal to use magnifying adaptors for imaging, because they lead to a loss of fluorescence signal in collection pathway. Hence this adaptor should be used only for convenience when observing with low-magnification objectives (20×) through the eyepieces.

High magnification lenses (40×, 60×, 100×) with higher numerical apertures provide images with higher spatial resolution in 3D. Using the "digital zoom" option available in majority systems for laser scanning microscopy, allows one to set the pixel size according to Nyquist. This kind of spatial sampling is not always necessary. For example, when imaging neuronal populations, we are interested mostly in the integrated signal from individual cells. Nyquist sampling, or even oversampling, is important if we ask questions about sub-resolution movements of small structures (i.e., quantitative analysis of spine movement). In this case, one should not consider a laser scanning microscope as an imaging device with resolution limit defined by diffraction, but more as a position-measuring instrument that measures the centroid of the distribution of fluorescent molecules and the dynamics of the position of this centroid.

For two-photon laser scanning microscopy, it is important to make sure that all the components of the excitation pathway have good transmission in the near IR. Users should use objective lenses corrected for optical distortions and made to be transparent in the NIR. In many cases, additional changes are needed in the installed optics to make them IR-transparent (pupil-transfer lens in our case; (Majewska *et al*., 2000b).

Objective lenses used for multi-photon imaging should be free of geometrical (spherical) aberrations. The requirement for the absence of chromatic aberrations is not so important — excitation light is practically monochromatic (the spectrum widening caused by the finite length of pulse from mode-locked lasers is negligible). Also, the absence of a confocal aperture in front of the detector and the general architecture of the collection system, emphasizes collecting the maximum fraction of the emitted light, and allows one the freedom of using collecting optics (objectives in case of 2P-fluorescence and condenser lens in the case of SHG) not well-corrected for chromatic aberration.

Beam Collimation and Pulse Broadening

The majority of modern microscopes are designed for infinity-corrected objective lenses, so it is important to provide collimated laser light to the back-aperture of the objective (Tsai and Kleinfield, 2002). Even if initially the microscope system and scanning head are designed to provide collimated light at the back-aperture of objectives, custom modifications of the optical pathway and the switch to NIR excitation can distort this collimation. This indeed happened in our custom-made 2P-microscope and we solved the problem by introducing additional optics into the excitation pathway (Nikolenko *et al.*, 2003). Specifically, we use a simple system of 2 lenses in order to collimate the light to the objective lens.

Our system also works as a "beam expander" — it modifies the laser beam in such a way that the excitation beam at the back aperture of objective is not only collimated, but also is large enough to slightly overfill the objective pupil. One of the major requirements for laser scanning microscopes is that the back aperture should be overfilled by the excitation light (Tsai and Kleinfield, 2002). This minimizes variation of excitation power across the field of view and guarantees that the full numerical aperture of the objective lens is used. The level of overfilling should be minimal to maximize the amount of excitation power deliveried to the sample.

Another important factor in 2P microscopy is the problem of pulse broadening. Nonlinear microscopy requires using pulsed laser light. Mode-locked lasers generate a train of pulses of finite length at certain repetition rate. Even though each pulse represents monochromatic light, the finite length of each pulse leads to a spectrum with certain width in Fourier-space. Linear dispersion of this light in the intermediate optical elements disturbs the phase relations between the different spectral components of the pulse, which in practice leads to the pulse being broadened in time. This decreases the peak excitation intensity, and hence decreases the efficiency of nonlinear excitation. In order to avoid this, the optical system should use the minimum number of lenses between the laser and the specimen. Alternatively, one can add additional optics with negative dispersion in order to compensate for the positive dispersion of the rest of the optics (Lechleiter *et al*., 2002).

Image Production, Resolution, and *z*-Sectioning

In our two-photon microscope, fluorescence is detected with photomultiplier tubes (PMTs; HC125-02, Hamamatsu, Japan) used in an external, whole-area detection mode, and images are acquired using Fluoview software (Olympus). Images are sometimes taken at the highest digital zoom, resulting in a nominal spatial resolution of 20–30 pixels per μm with the 40×. This spatial resolution is suitable for imaging very small structures including dendritic spines, the size of which is typically on the order of μm.

Since brain slices are three-dimensional, we collect a series of images (*z*-stack) from different focal planes to cover the whole neuronal structure of interest. In principle, three-dimensional structures can be reconstructed from the *z*-stack. However, this is not practical when the same structure is imaged repeatedly, particularly in time-lapse imaging, for the following reasons: (1) perfusion causes small movements of the slice so the reconstructed structures are not accurate and (2) to achieve pixelation in the *z*-direction at a similar level to the *x*- and *y*-direction, many focal planes have to be scanned. This is impractical because it compromises fast time-lapse imaging and increases the possibility of photodamage.

To circumvent these problems, we scan the images with a 1 μm difference between focal planes (up to 9 planes), and then project the *z*-stack into a single, two-dimensional image. Since the point spread function of the 60× objective lens in our microscope measures approximately 0.4 × 0.4 × 1.3 μm (Majewska *et al*., 2000b), the images with 1 μm focal distance have enough overlap to produce a good projection.

A major problem associated with time-lapse imaging of brain slices is slice movement in the *x*, *y* and *z*-directions. To minimize movement in *z*, we routinely scan extra focal planes at the top and the bottom of the *z*-stack. If movement in the structure of interest is evident in these extra focal planes, we move the whole *z*-stack 1 μm up or down. Thus, structures of interest are not lost from the *z*-stack. Structures of interest can also move out of the images by moving in the *x* or *y* directions. To minimize this, we try to make the slice adhere to the bottom glass of the chamber. In addition, we avoid placing the structures of interest near the edge of the image, and if the structures move near the edge, we reposition the specimen so that the structures move toward the center of the imaged area. Although this prevents the loss of structures of interest from the *z*-stack, *xy* movement results in the drift of the whole image in the time-lapse movies. In these movies, it is extremely difficult to observe and analyze changes in morphology and fluorescence intensity. Therefore, in the analysis we compensate the *xy* movement as described below.

Choice of Indicators for Two-Photon Imaging of Calcium

Two-photon excitation of calcium indicators loaded via whole-cell recording is ideal for imaging calcium during action potential generation or during synaptic excitation (Yuste and Denk, 1995). We have used both calcium green-1 and fluo-4 successfully and find that both indicators are excited well by a mode-locked laser at 800 nm. However, we find that each indicator is suited for different conditions. Because calcium green-1 is brighter at low calcium concentrations, it is ideally suited for visualizing fine structures such as dendritic spines. However, in part due to its high fluorescence at rest, its increase in intensity on binding calcium is compromised (F_{ca}/F_{free} = ~14), such that it is imperfect for detecting small or heavily buffered signals. On the other hand, although fluo-4 is dim at rest and therefore demands higher excitation laser power, it undergoes a large change in fluorescence on binding calcium (F_{max}/F_{min} = ~100). Thus, fluo-4 is ideal for imaging small or heavily buffered signals, such as in cortical interneurons, which have high endogenous buffering capacities. We have used calcium green-1 over the concentration range of 50 to 200 μ*M*, and fluo-4 from 100 to 400 μ*M*. Because increased indicator concentrations cause larger distortions of the true calcium signals, the smaller the concentrations yield more physiologically-relevant data; however, if higher laser intensities are necessary to observe signals in environments with low concentration, photodamage may be accelerated.

In our hands, indo-1 is the best choice when shorter wavelengths (<750 nm for two-photon excitation) are needed to combine calcium imaging with uncaging techniques. The two-photon sensitivity of calcium indicators is available from http://cellscience.bio-rad.com/products/multiphoton/Radiance2100MP/mpspectra.htm.

Photodamage

The Achilles' heel of all live imaging is phototoxicity. Using our two-photon microscope, we experience two types of photodamage, when imaging neurons with too-high laser power (>20 mW at the sample). First, unstained cells that show strong autofluorescence suddenly collapse, emitting high-intensity light, like an explosion. This often masks the structure of interest. We recommend not including any structures with high autofluorescence in the imaging area. Second, stable structures in labeled neurons can show abnormal morphological rearrangements, particularly beading. This type of photodamage is nonlinear and, in some cases, can start to occur even minutes after the illumination has stopped. Moreover, even though previous scans can be normal, the same intensity of excitation can suddenly cause photodamage, particularly if the imaged structures are near the surface of the slice and if the concentration of dye is high. As is the norm in all microscopy, we recommend imaging with as low an excitation intensity as possible and adjusting this intensity for each sample depending on the brightness of the image.

In some experiments where photodamage becomes a persistent problem, we use the antioxidant Trolox (Sigma, 10–100 μ*M*), added to the ACSF (Sheenen *et al*., 1996). We have not noticed any effect of Trolox on the physiology of the neurons, although it has been suggested that high concentrations of it can block NMDAR (A. Konnerth, personal communication).

Second Harmonic Imaging

Second harmonic generation (SHG) is a nonlinear optical effect in which the incident light is coherently scattered by the specimen at twice the optical frequency and at certain angles (Lewis *et al*., 1999; see Chapter 40, *this volume*). The signal can be produced by endogenous structures or from inserted chromophores. Unlike fluorescence, in which emitted photons are best detected in the epi configuration, SHG photons are best detected in the transmission path of the microscope. The SHG photons, generated at the focal spot of the laser in the sample, are collected by a condenser lens which has to have the same NA as the objective lens in order to collect the whole cone of light. This is important because the SHG radiation in the forward direction is restricted to certain off-axis angles. It is best to have a spatially filtered laser beam for SHG because it is a coherent process — the spatial filter acts as a point source and restores the Gaussian wavefront and phase. Spatial filtering can be achieved by a telescopic system of two positive lenses and a pinhole placed between them such that the pinhole-

to-lens distance equals the focal length, respectively. In front of the photomultiplier tube (PMT), which is placed in the transmission path, is a narrow band (~20 nm) filter centered at half the wavelength of the laser. The amplification of the signal is done by standard methods as in fluorescence detection. Specific instructions to adapt a two-photon microscope for SHG imaging can be found in Nikolenko and colleagues (2003).

Silicon-Intensified Target Camera Imaging

While two-photon imaging results in a high spatial resolution imaging with the least photobleaching and most depth penetration, there is a cost, as with any laser-scanning microscopy, in terms of temporal resolution when many neurons are simultaneously imaged because the laser beam must be systematically moved over a large area. While future scanning modifications may alleviate this problem, at present single-photon fluorescence imaging has proved a useful technique for measuring the fluorescence changes in several neurons simultaneously (Peterlin *et al*., 2000; Kozloski *et al*., 2001).

For example, using calcium imaging with fura-2, the typical detectable change in fluorescence that can be measured in a neuron from a single action potential has a fast onset (<100 ms rise time) and slow decay (>2 s; Smetters *et al*., 1999). This allows one to detect the time of occurrence of action potentials in identifiable neurons with 100 ms temporal resolution, provided that frames are acquired at a rate of 50 ms or less. We have achieved this using a SIT camera (Dage), BX50WI microscope (Olympus), 40× 0.8 NA water-immersion lens, an LG-3 frame grabber (Scion Corp.) in a Power Macintosh 7600, and NIH image software. With this equipment, we can view an area of cortex of 320 × 240 µm with a spatial resolution of 640 × 480 pixels, and we can capture frames at a rate of 30 frames/s. Using fura-2 AM loaded slices (see above for loading technique), we can image dozens of neuronal somata using a mercury source (Olympus), a 380 nm excitation filter and 510 nm emission filter. The gating of the light source is accomplished via a triggered shutter (Uniblitz), which fully opens in less than 30 ms after the triggering TTL pulse. The acquisition of a frame or a set of frames (a "movie") can also be initiated from an external trigger. The delay from triggering the movie to acquisition of fully illuminated frames is from 100 to 150 ms to compensate for the 100 to 150 ms lag of the camera. Each captured frame uses 307.3 kB of memory. Homemade macros have been written using NIH image, controlling the shutter through the modem port of the computer. These macros enable the acquisition of movies time-locked to either depolarizing current pulses in current-clamped neurons (as in Kozloski *et al*., 2001) or to a large PSC recorded in a voltage-clamped neuron via a window discriminator (WPI).

MORPHOLOGICAL PROCESSING AND ANALYSIS

As our most reliable method for morphological reconstructions, we use biocytin fills and processing to recover the morphologies of the neurons imaged (Fig. 41.4).

Biocytin Protocol

Following electrophysiological recordings, the slices are immediately placed in 4% paraformaldehyde in 0.12 *M* phosphate buffer (PB) and kept at 4°C overnight. Slices are then cryoprotected in 20% sucrose in 0.12 *M* PB for 2 to 8 h and frozen on dry ice in tissue freezing medium (catalog #H-TFM, Triangle Biomedical Sciences). Upon defrosting, slices are rinsed in 0.12 *M* PB three times and pretreated with 1% hydrogen peroxide in 0.12 *M* PB for 30 min under agitation at room temperature. The tissue is then rinsed in 0.02 *M* potassium phosphate saline (KPBS) and incubated in Avidin-Biotin-Peroxidase Complex (catalog #PK-6100, Vector Laboratories, Inc.) overnight under agitation at room temperature (10 µL solution A and 10 µL solution B per 1 mL of 0.02 *M* KPBS and 0.3% Triton-X). Slices are rinsed in 0.02 *M* KPBS three times and incubated in 0.7 mg/mL 3,3′-diaminobenzidine, 0.2 mg/mL urea hydrogen peroxide, 0.06 *M* Tris buffer (catalog #D-4293, Sigma-Aldrich) in 0.02 *M* KPBS for 5 to 15 min. Upon completed DAB reaction, the slices are rinsed in 0.02 *M* KPBS and mounted in Vectashield mounting medium (catalog #H-1000, Vector Laboratories, Inc.).

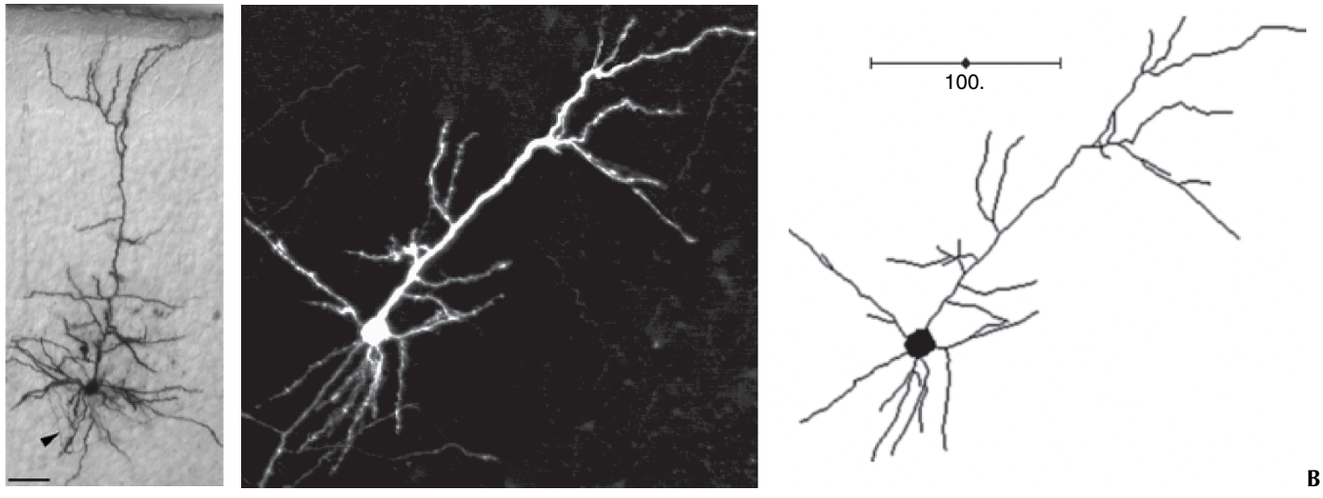

FIGURE 41.4. Histological reconstruction of neurons using biocytin and Neurolucida. (A) Biocytin staining. A pyramidal cell in a coronal section from mouse visual cortex was filled intracellularly with biocytin and then processed for visualization. Intracellular biocytin staining enables a large signal/noise and allows a fairly accurate reconstruction of the dendritic arbor of the neuron. Structures as small as spines (~1 µm in diameter) can be visualized. Arrowhead indicates the axon. Scale bar = 50 µm. (Courtesy of Z. Peterlin and A. Tsiola.) (B) Neurolucida reconstruction. (Left panel) Confocal image of a pyramidal neuron from a P7 mouse slice, cultured for 6 days. The cells were transfected with EGFP using a gene gun. (Right panel) Reconstruction of the neuron using Neurolucida.

Anatomy with a Two-Photon/Neurolucida System

We have experimented with direct two-photon reconstructions of the cells in the brain slices. This procedure enables the investigator to quickly reconstruct the morphology of the imaged cell. Images of neurons from both live and fixed tissue can be taken by the two-photon microscope and the stacks of images can be imported into a computerized reconstruction and measuring program, such as Neurolucida (Microbrightfield, Brattleboro, VT).

Two-Photon/Neurolucida Protocol

When examining dendritic morphology alone, *z*-stacks of the neuron of interest can be captured using a 20× or 40× objective. When spines and filopodia are also of interest, a 60× objective with a 2.5× digital zoom yields good images. For detailed reconstructions of the protrusions from the entire neuron, small overlapping sections of the neuron are imaged using the 60× objective and 2.5× digital zoom. After capturing the *z*-stack of images, they should be saved as a Fluoview Multi-Tiff (*.tiff) and transferred to a computer running the Neurolucida software. The images can either be burned onto a recordable CD, or can be transferred to the computer over a local area network.

The neurons can then be reconstructed using Neurolucida software. The stack can be opened using the Image Stack Open command under the File icon on the menu bar. Once the image is opened, the brightness and contrast of the image can be adjusted by selecting Image Effects under the Video icon. Once the picture is in clear focus, the neuron is ready to be reconstructed. The image must be calibrated and a reference point chosen. The PgUp and PgDn keys on the keyboard will allow for scrolling through the stack of images. The mouse is used to trace the neuron and the type of tracing can be set by right clicking on the image. We find that rubber line tracing is very effective. The thickness of the line can be determined by the scroll feature on the mouse (the wheel or center button). In the tool bar we are able to select the section of the neuron we are drawing, for example, apical dendrite or cell body. Nodes and branches are added by right clicking on the image during tracing. After the contour is completed, it can be saved and opened in the Neuroexplorer program. This program will allow for easy analysis of the reconstruction.

Correlated Electron Microscopy

Although we can image neuronal structures in live brain slices at quite high resolution with two-photon microscopy, for some questions, such as confirming the existence of a synapse, we find it necessary to use electron microscopy. We have pioneered the combination of two-photon live imaging with serial thin-section electron microscopy to enable us to examine the ultrastructure of dendritic spines and axonal filopodia (Dunaevsky *et al.*, 2001; Tashiro *et al.*, 2003).

Protocol for Two-Photon/Electron Microscopy Imaging of GFP-Labeled Cells

Neurons are transfected with eGFP using biolistics. Slices imaged with two-photon microscopy are fixed with 5% glutaraldehyde in PB for 1 h. The slices are then embedded in 3% agar and resectioned at 75 μm with a vibratome (Technical Products International, St. Louis). After locating the imaged neuronal structure in the sections using a fluorescence microscope, the sections are immunostained with anti-GFP antibody (Roche Diagnostics Corp.) overnight at 4°C, and then with peroxidase-conjugated goal anti-rabbit IgG antibody (Roche Diagnostics) for 1 h at room temperature. After developing with DAB, the sections are postfixed in 1% osmium tetroxide in PB, dehydrated, and then infiltrated with Epox 812 resin (Fullam), placed flat in resin between two plastic slides, and polymerized in the oven at 60°C. After polymerization, the plastic slides are separated and the imaged areas of interest were cut out, mounted on a blank block, and sectioned to 10 μm for examination under phase contrast. The 10 μm sections with the imaged areas of interest were then remounted on a blank block, thin sectioned, and examined in the electron microscope (JEM 1200EX). Imaged mossy terminals with filopodia are reconstructed from serial sections (see also Chapter 49, *this volume*).

Protocol for Two-Photon/EM Imaging of Biocytin Labeled Cells

Neurons are bolus injected with electrode containing 0.4% biocytin and 1 m*M* Alexa-488 as described before. Immediately after imaging, brain slices are immersion fixed with 4% paraformaldehyde and 0.5% glutaraldehyde in 0.1 *M* PB overnight at 4°C. They are washed three times 10 min on shaker at room temperature with 0.1 *M* PB. Then, slices are incubated in 1% hydrogen peroxide, 50% ethanol, and 0.05 *M* PB for 30 min at room temperature on shaker for eliminating internal peroxidase activity. After washing again, they are incubated with ABC (Vectastain) overnight at 4°C and 1 h at room temperature. After washing again, they are DAB reacted using fast DAB‰ from Sigma for about 3 min. Then, pictures are taken from the imaged region to facilitate its EM reconstruction. At this point, slices can be postfixed with glutaraldehyde. Finally, slices are osmicated by 1% osmium tetroxide together with 7% glucose and 0.005% $CaCl_2$. If there is a problem of revealing the imaged region with biocytin, slices can be resectioned after fixation. For this, slices are embedded in 3% agarose and resectioned using a vibratome. Freeze–thawing is another method to increase the penetration of reactants like ABC. For this, slices are kept in 30% sucrose until the slices sink to the bottom, and then dipped (in the plastic container with sucrose) into liquid nitrogen.

As a variant on this protocol, for fixing slices for EM, prepare a fix solution of 4% paraformaldehyde, 0.05% glutaraldehyde, and 15 mL of saturated picric acid in 100 mL of 0.1 *M* PB. Slice should be kept in this solution for approximately 3 h. Thereafter, slices may be stored in a solution of 0.05 *M* sodium azide in 0.1 *M* PB. Then follow the protocol above.

Morphological Classification of Neurons Using Cluster Analysis

One of the problems in classifying cortical neurons is their heterogeneity and the vast number of parameters that can be used for this purpose. These parameters usually encompass a massive array of physiological, morphological, and, most recently, gene expression data. A rigorous approach to classifying cortical neurons must involve a thorough analysis of the structure of the data before one attempts to assign neurons to certain clusters. Principal component analysis (PCA) and cluster analysis (CA) are valuable multivariate data analysis methods that can be used jointly with CA to address these issues (Kozloski *et al.*, 2001).

Protocol for PCA/CA

As a first step, we perform a PCA analysis using Statistica on the variables automatically measured by the Neurolucida program. In a second step, we perform cluster analysis (Wards's methods), also using Statistica.

Let $\boldsymbol{X}$ denote an $m \times n$ matrix of m cells (cortical neurons) with n measured or computed parameters. The elements of this matrix denoted by x_{ij} represent the value of the jth parameter for the ith neuron. For values of $n \leqslant 3$, visualization of data is impossible and thus the overall distribution of cells in their n-dimensional parameter space is not accessible. In the case of cortical neurons the number of dimensions can easily exceed tens or even hundreds with the inclusion of gene expression data. The major advantage of PCA methods is to help reconstruct a new parameter space with (optimally) three dimensions in such a way that it still faithfully represents the data with the minimum loss of information during the process of space transformation. This transformation involves computating eigenvalues (Σ) and eigenvectors (u) of the $n \times n$ correlation matrix ($\boldsymbol{R}$) of the original data matrix $\boldsymbol{X}$. The goal is to map the n-dimensional vector describing the parameters of each neuron to a vector with, for example, three dimensions, so that each neuron can be plotted in a three-dimensional (3D) graph. The desired new dimensions, also called principal factors or components, are extracted from the original space through the eigenvalue decomposition of the correlation matrix. This decomposition will provide the eigenvectors (principal components) and its related eigenvalue (total variance accounted for by each component). Principal component scores computed for each principal component give the coordinates of neurons in the reduced space. PCA methods also provide a matrix of factor or principal component loadings that show the correlation value of each original parameter with the newly computed components. These loading values show which parameters contribute significantly (highly positive or negative correlations) to the derived dimensions. It can be seen that, while some original parameters contribute significantly to some components, they contribute very little to others. Meanwhile, some original variables only contribute to principal components that carry a relatively low proportion of the total variance (low relative eigenvalue). These latter parameters are thus found to be less important in the characterization of the data structure.

The final stage of classification involves application of CA to the new coordinate values (principal component scores) of the neurons in the reduced space. Appropriate linkage rules for CA can be chosen based on the apparent shape of the clusters as seen in the scatter plot of neurons in the principal component space. Application of PCA before CA allows a rational choice of linkage rules which would lead to a better segregation of clusters.

IMAGE PROCESSING

Compensation for the Drift and the Vibration of the Slices

As described above, one of our problems is the movement of slices that produces the drift of images during long (>10 min) time-lapse movies. This drift of structures of interest makes it particularly difficult to observe and analyze changes in morphology and fluorescence intensity. Indeed, spine motility was only discovered in our laboratory after the alignment of time-lapse movies was performed (Dunaevsky *et al*., 1999). Therefore, we always compensate for the movement of slices.

Although manual alignment of time-lapse movies using the structures which are always stable as references works well, this is time consuming. Instead, we have been using three automatic methods of alignment. Two of them are custom-made programs based on the overlap between the images and the center of mass, respectively. These programs are written in NIH image and ImageJ software, respectively. The other is commercially available software from AutoQuant Imaging, Inc.

Alignment Based on the Overlap Between Images

This alignment program is written as an NIH image macro. The principle of this macro is quite simple. Take two images, project these two images, and compare the average pixel values of the projected image and the original image. The more similar the two original images are and the more overlap they have, the closer the two average pixel values will be.

Protocol for Overlap Alignment

Before performing automatic alignment, images are thresholded to highlight neuronal structures. Ideally, the original images should work as well. However, because optical noise changes during time-lapse sequences, in practice, thresholded images work better. The macro selects two images and performs multiple iterations of an alignment procedure using the above principle. Each iteration comprises shifting the second original image by 1 to a certain number of pixels in four directions (up, down, left, right), comparing the average pixel values of the projected images and the first image, determining the optimal shift, where the average pixel values of the projected image and the original image are closest, and moving the second image by this optimal shift. From the second iteration on, images are only shifted in three directions because one of four directions is toward a starting point to the previous iteration. To avoid including the blank peripheral area which arises from the shift of the second image, only the area where the first original image and the shifted second image overlap are used to calculate the average pixel values of the projected image and the first original image. These iterations are repeated until an iteration finds that the original position of the second image in the iteration is optimal, or, in other words, the average pixel values of the projected image and the original image are closest in the ending position of the iteration.

This alignment macro works very well for most time-lapse sequences of projected images when the images have more area with stable structures than with unstable ones. For example, in the case of the time-lapse imaging of dendritic spine motility, the morphological changes in spines are quite small compared to the stability of the much larger dendritic shafts. Thus, in most cases, the alignment macro works reasonably well. When, in rare cases, alignment does not work completely, we align the movies manually using NIH image software.

We use this alignment for z-stacks where the structure of interest shifts between focal planes because of slice movement. Images in z-stacks are not aligned as well as time-lapse movies consisting of projected images since each image in a z-stack is different from the next image (with small overlapping). Although not ideal, the same macro helps to align z-stacks. We check all aligned stacks and correct them manually if the alignment is not good.

Alignment Based on the Center of Mass

We have created a different alignment program as a plug-in for ImageJ software using Java programming language. This program is based on the calculating relative positions of the center of mass of the drifting objects.

Protocol for Center of Mass Alignment

The coordinates of center of mass are calculated by using the pixel value as a mass. For meaningful calculations, a cut-off value is used in order to prevent including background pixels in the calculation. Our program calculates the center of the first frame in the image stack and uses these coordinates as the reference point for aligning the rest of the image stack (i.e., It considers the first frame as not drifted).

The program then calculates coordinates of the center of mass of the each image in the stack. The program then shifts each image in order to align images in such a way that centers of mass of all frames have the same coordinates (they overlap each other).

If a region of interest (ROI) is chosen, the program aligns to the center of mass of the ROI. The ROI can be any shape and allows aligning by using center of mass of a selected object, not whole image.

This algorithm is quite simple, fast, and works well if the center of mass is always calculated from the same structure. However, drift of the slices can make a new structure appear or a part of a structure disappear from the edge of the image. Because this edge effect can make the center of mass move to completely different positions in different images, purely automatic alignment is sometimes unsuccessful. On the other hand, choosing a stable structure as the ROI for alignment can prevent this artifact.

The next logical step in the development of this type of algorithm could be using spatial moments of higher order (center mass coordinates are spatial moments of the first order; and the total mass is spatial moment of zero order). For example, including in the alignment algorithm, spatial moments of the second order and third order will allow compensating not only for drift, but also for image rotation and squeezing.

Online Cell Detection of Neurons

Using AM loading, we can simultaneously image over 3000 neurons (Fig. 41.3). To analyze fluorescence changes, such as those indicating Ca^{2+} concentration, of a large number of individual cells, we need to identify and select all the neurons. As manual selection of this many cells is quite tedious and cannot be performed online, automatic cell detection algorithms were developed in ImageJ (NIH, Bethesda, MD) and Matlab (MathWorks, Natick, MA) [Fig. 41.5(A)].

Protocol for Center of Mass Alignment

First, time-lapse movies are collapsed in time, creating a single projected image by averaging the fluorescence of each pixel throughout the recording. This effectively reduces the amount of spatial noise in the image and reveals smaller elements, such as dendrites. Due to the slightly unequal loading of different regions

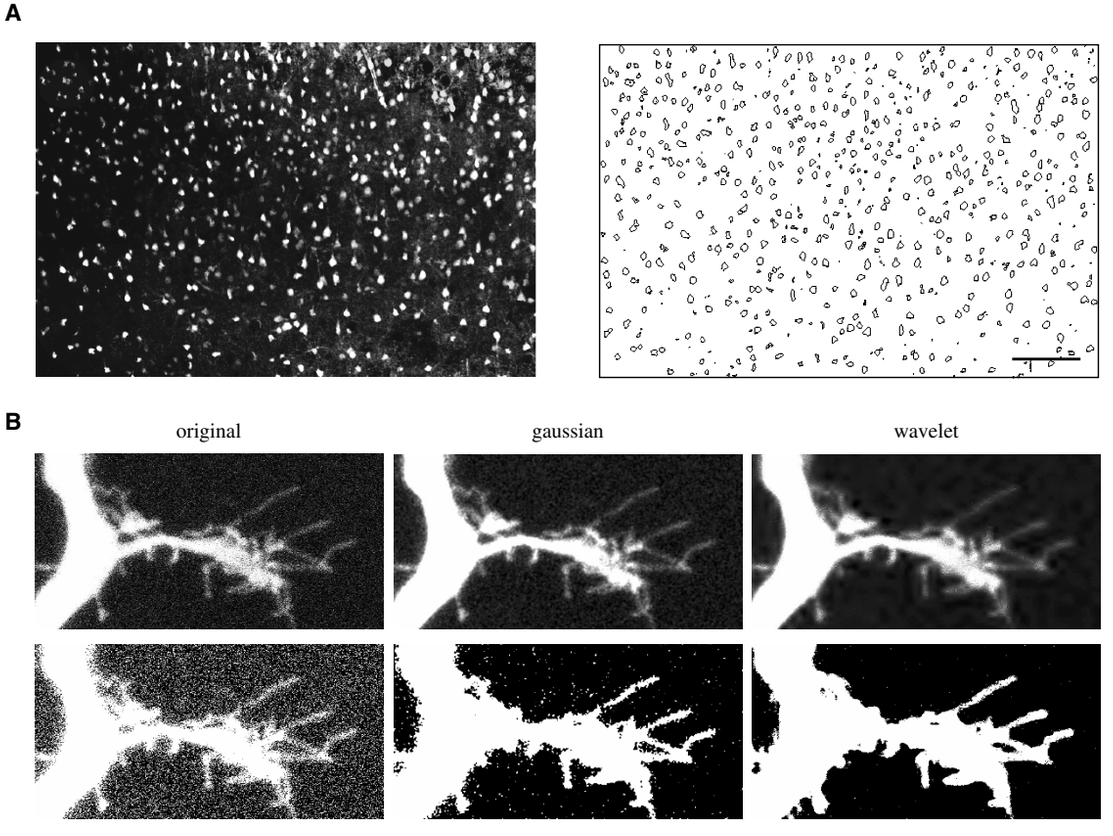

FIGURE 41.5. Image processing algorithms. (A) Cell detection algorithm. (Left) An original image of a fura-2 loaded acute slice. Note how the staining is not even throughout the image. (Right) An image with outlines of all detected cells. The contours of the cells are drawn. (B) De-noising algorithms. (Upper panels) Images of a dendritic growth cone from a cortical pyramidal neuron. All three images are shown with the same brightness and contrast. (Lower panels) Binarized images. All three images are thresholded with the same pixel value. (Left) Original images. (Center) Gaussian-filtered images. (Right) Images de-noised with wavelet transformation.

of the slice, the average fluorescence level of cells in the same slice often vary, making automatic detection problematic. To account for these spatial fluorescence variations, the value of each pixel is normalized, dividing it by the average fluorescence of a 25 × 25 µm square centered at that pixel. In the resulting image, the fluorescence level is almost constant for all cells and is typically between 1.2 and 1.5. Contours can be plotted at a manually chosen value in this range using the Matlab contour drawing algorithm. Every closed contour corresponds to the accurately detected boundary of a fluorescent entity in the imaged field. This method identifies practically all cells, as well as a large number of smaller non-cellular elements in the slice [Fig. 41.3(A)]. By measuring the average fluorescence value of the pixels inside each contour as a function of time, we can quickly reconstruct fluorescence changes of large populations with single-cell resolution. In total, this allows us to measure calcium fluorescence signals from roughly 400 to 1400 entities per slice.

Image De-Noising Using Wavelets

The external PMT in our two-photon system produces uncorrelated dark noise, primarily of thermal origin. This type of noise has a strong dependence on applied bias voltage (Majewska *et al*., 2000b; www.twophoton.com). It is therefore important to correctly choose the bias voltage in order to balance the resulting gain of the PMT versus noise.

This type of noise is intrinsically random and does not have specific spectral components. Therefore, it cannot be distinguished from the real signal by classic methods of linear filtration. For example, the widely used mean and Gaussian windows filters are not efficient in terms of removing this type of noise (Fig. 41.5). Indeed, background noise removal is very important for quantitative analysis of thresholded images, and linear filtration of noisy images usually gives artifacts [Fig. 41.5(B)].

As an alternative approach, we use wavelet transformation for the purpose of image de-noising (Lio, 2003). Wavelet transformation is widely used for signal compression and de-noising and represents further development of classic methods of analysis such as Fourier, Gabor, and short-time Fourier transformation. The wavelet transformation gives full representation of the signal [for one-dimensional (1D) time signals, a correct representation in time and frequency domains; for two-dimensional (2D) images, a representation of spatial frequencies and coordinates]. Whereas Fourier transformation presumes the infinite dimensions of the image space, wavelet transformation is inherently local and gives a better representation of naturally occurring finite-size objects in image.

Protocol for Wavelet De-Noising

The general de-noising procedure consists of the following steps:

In case of image de-noising, an individual image is represented as 2D array of numbers (pixel values). The wavelet transformation decomposes this 2D signal into wavelet space by using a specified wavelet family. In case of discrete wavelet transformations, it computes the detail coefficient of the signal up to the certain predefined level. For the purpose of signal de-noising, the detail coefficients at all levels of decomposition have to be thresholded. The numerical value of the threshold can be chosen based on the noise model used.

There are several methods of thresholding. The practical choice of the method depends on the nature of the signal and the chosen model. Reverse wavelet reconstruction is then performed using the modified detail coefficients, and the filtered image is regenerated from thresholded detail coefficients by using the inverse wavelet transformation.

The latest release of the Wavelet Toolbox (version 2.2) for Matlab (The MathWorks Inc., Natick, MA) provides a variety of ready-to-use tools for wavelet transformation and signal de-noising. There is an interactive graphical user interface in Wavelet Toolbox, which simplifies the task of choosing the parameters for signal de-noising and compression. In the simplest case, practical de-noising can be done based on the visual perception of the de-noising quality, but also using different recovery criteria (e.g., based on entropy estimation).

For large-scale image processing, we created a custom code in Matlab, which performs simple image de-noising based on the chosen model. As a model, we use wavelet decomposition to level 4 with symlet-6 wavelets, and soft thresholding (see more theory of de-noising procedure in Wavelet Toolbox documentation). The script processes raw images in a multi-TIFF format, gives acceptable de-noising, and does not change the quantitative values of intensity in the principal image details [see Fig. 41.3(B)]. Our algorithm processes each frame individually, therefore processing time depends linearly on the size of the image stack. The algorithm is not memory demanding and turned out to be relatively fast — it takes approximately 5 s to process a 800 × 600 pixel, 16-bit image on a 1.9 GHz Pentium 4 PC.

SUMMARY

- Brain slices are convenient preparations because they permit the easy manipulation of their environment, access for imaging or electrophysiological equipment, and preservation of three-dimensional organization of the brain region studied.
- We describe the techniques of live-slice imaging we use in our laboratory, including slice preparation (acute and cultured slices), cell labeling (biolistics, diolistic, calistics, injection with patch electrodes, and AM loading), morphological processing and analysis, imaging procedures (two-photon, second harmonic, and camera imaging), and image processing.
- Although *in vivo* imaging techniques have recently developed in many species, brain-slice imaging has advantages for studying many questions and will be increasingly important for cortical research.

ACKNOWLEDGMENTS

We thank the National Eye Institute (EY11787 and EY13237), the NINDS (NS40726), the New York STAR Center for High Resolution Imaging of Functional Neural Circuits, the HFSP, and the John Merck Fund for their support.

REFERENCES

Agmon, A., and Connors, B.W., 1991, Thalamocortical responses of mouse somatosensory (barrel) cortex *in vitro*, *Neuroscience* 41:365–379.

Alger, B.E., Dhanjal, S.S., Dingledine, R., Garthwaite, J., Henderson, G., King, G.L., Lipton, P., North, A., Schwartzkroin, P.A., Sears, T.A., Segal, M., Whittingham, T.S., and Williams, J., 1984, Brain slice methods, In: *Brain Slices* (R. Dingledine, ed.), Plenum Press, New York, pp. 381–437.

Arnold, D., Feng, L., Kim, J., and Heintz, N., 1994, A strategy for the analysis of gene expression during neural development, *Proc. Natl. Acad. Sci. USA* 91:9970–9974.

Beierlein, M., Fall, C.P., Rinzel, J., and Yuste, R., 2002, Thalamocortical bursts trigger recurrent activity in neocortical networks: Layer 4 as a frequency-dependent gate, *J. Neurosci.* 22:9885–9894.

Brenner, S., 2002, Life sciences: Detective rummages, investigates, *The Scientist*, 16(6):15–16.

Dunaevsky, A., Blazeski, R., Yuste, R., and Mason, C., 2001, Spine motility with synaptic contact, *Nat. Neurosci*. 4:685–686.

Dunaevsky, A., Tashiro, A., Majewska, A., Mason, C.A., and Yuste, R., 1999, Developmental regulation of spine motility in mammalian CNS, *Proc. Natl. Acad. Sci. USA* 96:13438–13443.

Edwards, F.A., Konnerth, A., Sakmann, B., and Takahashi, T., 1989, A thin slice preparation for patch recordings from neurones of mamalian central nervous system, *Pflugers Arch*. 414:600–612.

Feng, G., Mellor, R.H., Bernstein, M., Keller-Peck, C., Nguyen, Q.T., Wallace, M., Nerbonne, J.M., Lichtman, J.W., and Sanes, J.R., 2000, Imaging neuronal subsets in transgenic mice expressing multiple spectral variants of GFP, *Neuron* 28:41–51.

Franklin, K.B.J., and Paxinos, G., 1997, *The mouse brain in stereotaxic coordinates*, Academic Press, San Diego, California.

Gan, W.B., Grutzendler, J., Wong, W.T., Wong, R.O., and Lichtman, J.W., 2000, Multicolor "DiOlistic" labeling of the nervous system using lipophilic dye combinations, *Neuron* 27:219–225.

Grynkiewicz, G., Poenie, M., and Tsien, R.Y., 1985, A new generation of Ca^{2+} indicators with greatly improved fluorescence properties, *J. Biol. Chem*. 260:3440–3450.

Helmchen, F., Imoto, K., and Sakmann, B., 1996, Ca2+ buffering and action potential-evoked Ca2+ signalling in dendrites of pyramidal neurons, *Biophys. J.* 70:1069–1081.

Honig, M.G., and Hume, R.I., 1989, DiI and DiO: Versatile fluorescent dyes for neuronal labelling and pathway tracing, *Trends Neurosci*. 334:333–340.

Kettunen, P., Demas, J., Lohmann, C., Kasthuri, N., Gong, Y., Wong, R.O., and Gan, W.B., 2002, Imaging calcium dynamics in the nervous system by means of ballistic delivery of indicators, *J. Neurosci. Methods* 119:37–43.

Kozloski, J., Hamzei-Sichani, F., and Yuste, R., 2001, Stereotyped position of local synaptic targets in neocortex, *Science* 293:868–872.

Lechleiter, J.D., Lin, D.T., and Sieneart, I., 2002, Multi-photon laser scanning microscopy using an acoustic optical deflector, *Biophys. J*. 83:2292–2299.

Lewis, A., Khatchatouriants, A., Treinin, M., Chen, Z., Peleg, G., Friedman, N., Bouevitch, O., Rothman, Z., Loew, L., and Sheves, M., 1999, Second harmonic generation of biological interfaces: Probing membrane proteins and imaging membrane potential around GFP molecules at specific sites in neuronal cells of *C. elegans*, *Chem. Phys*. 245:133–144.

Lio, P., 2003, Wavelets in bioinformatics and computational biology: state of art and perspectives, *Bioinformatics* 19:2–9.

Lo, D.C., McAllister, A.K., and Katz, L.C., 1994, Neuronal transfection in brain slices using particle-mediated gene transfer, *Neuron* 13:1263–1268.

Lohmann, C., Myhr, K.L., and Wong, R.O., 2002, Transmitter-evoked local calcium release stabilizes developing dendrites, *Nature* 418:177–181.

Majewska, A., Tashiro, A., and Yuste, R., 2000a, Regulation of spine calcium compartmentalization by rapid spine motility, *J. Neurosci*. 20:8262–8268.

Majewska, A., Yiu, G., and Yuste, R., 2000b, A custom-made two-photon microscope and deconvolution system, *Eur. J. Physiol*. 441:398–409.

Nikolenko, V., Nemet, B., and Yuste, R., 2003, A custom two-photon and second harmonic microscope, *Methods*. 30(1):3–15.

Peterlin, Z.A., Kozloski, J., Mao, B., Tsiola, A., and Yuste, R., 2000, Optical probing of neuronal circuits with calcium indicators, *Proc. Natl. Acad. Sci. USA* 97:3619–3624.

Sheenen, W.J.J.M., Makings, L.R., Gross, L.R., Pozzan, T., and Tsien, R.Y., 1996, Photodegration of indo-1 and its effect on apparent Ca concentrations, *Chem. Biol*. 3:765–774.

Smetters, D.K., Majewska, A., and Yuste, R., 1999, Detecting action potentials in neuronal populations with calcium imaging, *Methods* 18:215–221.

Tashiro, A., and Yuste, R., 2004, Regulation of dendritic spine motility and stability by Rac1 and Rho kinase: evidence for two forms of spine motility, *Mol. Cell Neurosci.* 26(3):429–440.

Tashiro, A., Dunaersky, A., Blazeski, R., Mason, C.A., and Yuste, R., 2003, Bidirectional regulation of hippocampal mossy fiber filopodial motility in kainate receptors: a two-step model of synaptogenesis, *Neuron*, 38(5):773–784.

Tashiro, A., Minden, A., and Yuste, R., 2000, Regulation of dendritic spine morphology by the Rho family of small GTPases: Antagonistic roles of Rac and Rho, *Cerebral Cortex* 10:927–938.

Tsai, P.S., Nishimura, N., Yoder, E.J., White, A., Doluick, E., and Kleinfeld, D., 2002, Principles, design and construction of a two-photon scanning microscope for *in vitro* and *in vivo* studies, in Methods for *in vivo* Optical Imaging (R. Frostig, ed.), CRC Press, pp. 113–171.

Tsien, R.Y., 1989, Fluorescent probes of cell signaling, *Ann. Rev. Neurosci*. 12:227–253.

Tsiola, A., and Yuste, R., 2003, Classification of neurons in the mouse primary visual cortex, *J. Comp. Neurol*. 461(4):415–428.

Yuste, R., 2000a, Loading populations neurons in slices with AM calcium indicators, In: *Imaging Neurons: A Laboratory Manual* (R. Yuste, F. Lanni, A. Konnerth, eds.), Cold Spring Harbor Press, Cold Spring Harbor, New York, pp. 34.31–34.39.

Yuste, R., 2000b, *Imaging Neurons: A Laboratory Manual*, Cold Spring Harbor Press, Cold Spring Harbor, New York.

Yuste, R., and Denk, W., 1995, Dendritic spines as basic units of synaptic integration, *Nature* 375:682–684.

Yuste, R., and Katz, L.C., 1989, Transmitter-induced changes in intracellular free calcium in brain slice of developing neocortex, *Soc. Neurosci. Abstr*. 4.5:2.

Yuste, R., and Katz, L.C., 1991, Control of postsynaptic Ca2+ influx in developing neocortex by excitatory and inhibitory neurotransmitters, *Neuron* 6:333–344.

Zilles, K., and Wree, A., 1985, Cortex: A real and laminar structure, In: *The Rat Nervous System* (G. Paxinos, ed.), Academic Press, Sydney, pp. 375–415.